

Detecting supernova neutrinos with iron and lead detectors

Abhijit Bandyopadhyay,^{1,*} Pijushpani Bhattacharjee,^{2,†} Sovan Chakraborty,^{3,4,‡} Kamales Kar,^{1,§} and Satyajit Saha^{2,¶}

¹*Ramakrishna Mission Vivekananda University, Belur Math, Howrah 711202, India*

²*Saha Institute of Nuclear Physics, 1/AF Bidhannagar, Kolkata 700064, India*

³*Department of Physics, Indian Institute of Technology - Guwahati, Guwahati 781039, India*

⁴*Max-Planck-Institut für Physik (Werner-Heisenberg-Institut), Föhringer Ring 6, 80805 München, Germany*

Supernova (SN) neutrinos can excite the nuclei of various detector materials beyond their neutron emission thresholds through charged current (CC) and neutral current (NC) interactions. The emitted neutrons, if detected, can be a signal for the supernova event. Here we present the results of our study of SN neutrino detection through the neutron channel in ^{208}Pb and ^{56}Fe detectors for realistic neutrino fluxes and energies given by the recent Basel/Darmstadt simulations for a 18 solar mass progenitor SN at a distance of 10 kpc. We find that, in general, the number of neutrons emitted per kTon of detector material for the neutrino luminosities and average energies of the different neutrino species as given by the Basel/Darmstadt simulations are significantly lower than those estimated in previous studies based on the results of earlier SN simulations. At the same time, we highlight the fact that, although the total number of neutrons produced per kTon in a ^{56}Fe detector is more than an order of magnitude lower than that for ^{208}Pb , the dominance of the flavor blind NC events in the case of ^{56}Fe , as opposed to dominance of ν_e induced CC events in the case of ^{208}Pb , offers a complementarity between the two detector materials so that simultaneous detection of SN neutrinos in a ^{208}Pb and a sufficiently large ^{56}Fe detector suitably instrumented for neutron detection may allow estimating the fraction of the total μ and τ flavored neutrinos in the SN neutrino flux and thereby probing the emission mechanism as well as flavor oscillation scenarios of the SN neutrinos.

I. INTRODUCTION

Detection of the neutrinos emitted during core collapse supernova (SN) explosion events is important for two reasons. Firstly, these neutrinos carry information about the core of the exploding star whereas no other particle or radiation can come out of that very high density region. Secondly, the properties of neutrinos like their mass hierarchy and flavor mixing, and their charged and neutral current interactions with matter inside the supernova may leave some imprints on the number of neutrinos detected and their temporal structure [1, 2], thereby allowing those neutrino properties as well as the core collapse supernova explosion mechanism to be probed. Because of these reasons a number of detectors capable of detecting SN neutrinos have come into operation during the past twenty five years or so after the detection of neutrinos from supernova 1987A located in the Large Magellanic Cloud at a distance of ~ 50 kpc [3–6]. For a recent review of the capabilities and detection methods of currently operating as well as near-future and proposed future SN neutrino detectors, see Ref. [7].

In this paper we study the possibility of detection of SN neutrinos with iron or lead as detector materials through detection of neutrons emitted from the nuclei excited by

the SN neutrinos. The use of such heavy-nuclei materials for detection of SN neutrinos through the neutron channel has been discussed by a number of authors in the past [8–10]. In general, neutron rich nuclei offer good sensitivity to ν_e 's through charged current (CC) process $\nu_e + n \rightarrow p + e^-$ in contrast to water Cerenkov or organic scintillator based detectors which are primarily sensitive to $\bar{\nu}_e$'s through the CC inverse beta decay process $\bar{\nu}_e + p \rightarrow n + e^+$. Further, CC cross section for ν_e interaction with high Z nuclei receives significant enhancement due to Coulomb effect on the emitted electron, and correlated nucleon effect also amplifies the ν -nucleus cross section relative to ν -nucleon cross section as a function of A . In particular, ^{208}Pb — it being both a highly neutron rich ($N = 126$) as well as high $Z (= 82)$ nucleus — is considered a good material for detection of the ν_e 's from SN through the CC reaction $\nu_e + ^{208}\text{Pb} \rightarrow e^- + ^{208}\text{Bi}^*$, with the excited $^{208}\text{Bi}^*$ nucleus ($N = 125, Z = 83$) subsequently decaying by emitting one or more neutrons. For a recent detailed study of the effectiveness of ^{208}Pb as a SN neutrino detector material, done within the context of the currently operating HALO [11] detector, see Ref. [12].

A ^{208}Pb detector would, of course, also be sensitive to all the six ν and $\bar{\nu}$ species including $\nu_\mu, \bar{\nu}_\mu, \nu_\tau,$ and $\bar{\nu}_\tau$ components through neutral current (NC) interaction $\nu(\bar{\nu}) + ^{208}\text{Pb} \rightarrow \nu(\bar{\nu}) + ^{208}\text{Pb}^*$, with the excited $^{208}\text{Pb}^*$ nucleus subsequently decaying by emitting one or more neutrons. However, the ν - ^{208}Pb NC cross section in the SN neutrino energy range of interest is typically a factor of 20 or so smaller than the ν_e - ^{208}Pb CC cross section [9], and even considering equal contributions from

*Electronic address: abhijit@rkmvu.ac.in

†Electronic address: pijush.bhattacharjee@saha.ac.in

‡Electronic address: sovan@iitg.ac.in

§Electronic address: kamales.kar@gmail.com

¶Electronic address: satyajit.saha@saha.ac.in

all six ν plus $\bar{\nu}$ species, the total number of interactions would be expected to be dominated by those due to the ν_e CC interactions; see, e.g., Ref. [12]. Indeed, our calculations below show that the neutrons from NC interactions would comprise $\sim 20\%$ or less of all events in a ^{208}Pb detector. On the other hand, a material with $N \approx Z$, such as ^{56}Fe ($N = 30, Z = 26$), while being significantly less neutron rich compared to ^{208}Pb and thus having a ν_e CC cross section more than an order of magnitude less than that for ^{208}Pb in the relevant SN neutrino energy range of interest, the flavor blind ν - ^{56}Fe NC cross section is less than the corresponding ν_e - ^{56}Fe CC cross section only by a factor of ~ 4 -5. With six species of ν plus $\bar{\nu}$ contributing roughly equally, the total number of interactions in a ^{56}Fe detector may be expected to be dominated by NC interactions. Indeed, this expectation is borne out by our calculations below, which show that $\sim 60\%$ or more of the total number of neutrons in a ^{56}Fe detector would come from NC interactions as compared to $\sim 20\%$ or less in a ^{208}Pb detector. Thus, an appropriately large ^{56}Fe detector can be a good NC detector for SN neutrinos. In this respect, in absence of separate identification of the CC events, simultaneous detection of SN neutrinos in a ^{208}Pb and a ^{56}Fe detector, for example, can, in principle, provide an estimate of the fraction of the $\nu_\mu, \bar{\nu}_\mu, \nu_\tau$ and $\bar{\nu}_\tau$ components in the total SN ν flux, thereby probing the emission as well as flavor oscillation scenarios of SN neutrinos.

Motivated by the above considerations, in this paper we make a comparative study of the efficacies of the two materials, ^{56}Fe and ^{208}Pb , as detector materials for SN neutrinos. In doing this, differing from previous studies, we use the results of the most recent state-of-the-art Basel/Darmstadt (B/D) simulations [13] for the supernova neutrino fluxes and average energies, which typically yield closer fluxes among different neutrino flavors and lower average energies compared to those given by earlier simulations (see, e.g., [14, 15]). The B/D models are based on spherically symmetric general relativistic hydrodynamics including spectral three-flavor Boltzmann neutrino transport. These simulations are much more realistic compared to the earlier simulations based on simple leakage schemes [14] without full Boltzmann neutrino transport. The lower average energies of the different neutrino species in the B/D simulations are related to the significantly larger radii of the neutrinospheres of the different neutrino species found in the new simulations as compared to those in the previous simulations. Indeed, several recent investigations with the full Boltzmann transport equation and their consecutive upgrades (e.g., Ref. [16]) have also consistently shown colder neutrino fluxes compared to the earlier SN simulations. As a consequence, as we shall see below, our results for the number of neutrons emitted are, in general, significantly lower than those obtained previously.

We note here in passing that recently an additional avenue of flavor independent detection of all six species of SN neutrinos has opened up with the advent of very

low threshold Dark Matter (DM) detectors which are primarily designed to detect the Weakly Interacting Massive Particle (WIMP) candidates of DM through detection of nuclear recoil events caused by the scattering of WIMPs from nuclei of the chosen detector materials (see, for example, the recent review [17]). Because of their capability to detect very low ($\sim \text{keV}$) energy nuclear recoils, such detectors would be sensitive to nuclear recoils caused by coherent elastic neutrino-nucleus scattering ($\text{CE}\nu\text{NS}$) of the relatively low energy ($\sim \text{few MeV}$) SN neutrinos of all flavors [18] with the cross section for the process roughly proportional to N^2 [19], where N is the neutron number of the detector material. These DM detectors, being also potential NC detectors of SN neutrinos of all flavors, may thus provide important information about the SN neutrino flux complementary to those derived from conventional (mostly CC) SN neutrino detectors. For recent studies on this topic, see, e.g., [20–22]. This, however, is beyond the scope of the present paper and will not be further discussed here.

The rest of this paper is arranged as follows: In Section II we briefly describe neutrino emission from core collapse supernovae and the basic results of the B/D simulations for a typical explosion of a $18M_\odot$ star. Section III discusses the CC and NC cross sections for interaction of neutrinos with lead and iron nuclei and the process of emission of neutrons from these nuclei. The number of neutrons emitted as a function of the neutrino energy is calculated by folding in the one-, two- and three neutron emission probabilities (as functions of the excitation energies of the nucleus under consideration) with the differential cross section for neutrino induced excitation of the nucleus to different excitation energies. Section IV gives the results for the number of neutrons emitted and makes a comparative study between lead and iron as detector materials. The paper ends with a summary and conclusions in Section V.

II. NEUTRINOS FROM CORE COLLAPSE SUPERNOVAE

The current understanding of neutrino emission from a typical core collapse SN event is that it occurs in three main phases. For the first 25 – 30 ms post bounce, there is a burst of electron neutrinos (ν_e) due to rapid deleptonization ($p + e^- \rightarrow n + \nu_e$) in the core. This neutronization burst phase is followed by the accretion phase, lasting for a few hundred ms, when neutrinos and antineutrinos of all flavors are emitted. These accretion phase neutrinos are powered by the gravitational energy released by the in-falling material accreting on to the central object. Finally, at the end of the accretion phase the shock (responsible for the SN event) breaks through the mantle of the star and the cooling phase ensues when neutrinos and antineutrinos of all three species of neutrinos are emitted. The cooling phase is the longest one, lasting for about 10 seconds, during which the bulk of

the total explosion energy is emitted in the form of neutrinos. The neutrino production in these different phases depends on different nuclear processes, the energetics of the phase and size of the progenitor core. Thus the luminosities and average energies of these neutrinos vary from one phase to another.

To estimate the total neutrino flux as a function of energy on a detector at Earth, one needs the energy spectra of the emitted neutrinos and their luminosities in the different phases. The number of primary (i.e., at the neutrinosphere) neutrinos of flavor i ($\nu_i \equiv \nu_e, \bar{\nu}_e, \nu_x, \bar{\nu}_x$, with ν_x representing ν_μ or ν_τ) emitted per unit time per unit energy is in general written as

$$F_{\nu_i}^0(t, E_\nu) = \frac{L_{\nu_i}(t)}{\langle E_{\nu_i} \rangle(t)} \varphi_{\nu_i}(E_\nu, t), \quad (1)$$

where $L_{\nu_i}(t)$ and $\langle E_{\nu_i} \rangle(t)$ are the time dependent luminosity and average energy of the emitted neutrinos of flavor ν_i , and $\varphi_{\nu_i}(E_\nu, t)$ is the instantaneous normalized energy spectrum ($\int \varphi_{\nu_i}(E_\nu, t) dE_\nu = 1$), which can be parametrized as [23]

$$\begin{aligned} \varphi_{\nu_i}(E_\nu, t) &= \frac{1}{\langle E_{\nu_i} \rangle(t)} \frac{(1 + \alpha_{\nu_i}(t))^{1 + \alpha_{\nu_i}(t)}}{\Gamma(1 + \alpha_{\nu_i}(t))} \left(\frac{E_\nu}{\langle E_{\nu_i} \rangle(t)} \right)^{\alpha_{\nu_i}(t)} \\ &\times \exp \left[- \left(1 + \alpha_{\nu_i}(t) \right) \frac{E_\nu}{\langle E_{\nu_i} \rangle(t)} \right], \quad (2) \end{aligned}$$

where

$$\alpha_{\nu_i}(t) = \frac{2\langle E_{\nu_i} \rangle^2(t) - \langle E_{\nu_i}^2 \rangle(t)}{\langle E_{\nu_i}^2 \rangle(t) - \langle E_{\nu_i} \rangle^2(t)}$$

is the spectral shape parameter. We will loosely refer to the quantity F^0 as the ‘‘flux’’ with the understanding that the actual flux at Earth will be obtained by dividing the final emerging number of neutrinos from the SN per unit time and energy by $4\pi d^2$, d being the distance from the Earth to the SN (assumed to be 10 kpc in the numerical calculations). For benchmark values of the quantities $L_{\nu_i}(t)$, $\langle E_{\nu_i} \rangle(t)$ and $\langle E_{\nu_i}^2 \rangle(t)$ we use those obtained from the results of the hydrodynamic simulations of the B/D group [13] for a $18M_\odot$ progenitor star. These values are extracted for each time bin of the simulation and then time integrated to get the total flux. The variation of the luminosity and average energy over the emission time and the time-averaged normalized energy spectra of neutrinos of different flavors are shown in Figure 1. Note that all the ν_x and $\bar{\nu}_x$ have the same luminosities, average energies and spectra in the B/D simulations.

The neutrinos of different flavors emitted from their respective neutrinospheres can undergo a variety of flavor oscillation scenarios in passing through the SN matter. Unlike in many other neutrino sources, neutrinos and antineutrinos of all three flavors are present in core collapse SN explosions. This can give rise to interesting flavor oscillation scenarios. In addition, the extreme neutrino densities in the deep interior (first few hundred

km) of SN can trigger collective neutrino oscillations due to neutrino-neutrino interactions; see, e.g., Refs. [24, 25] for reviews and references. While diffusing out of the exploding star these neutrinos will also go through the conventional Mikheyev-Smirnov-Wolfenstein (MSW) flavor oscillation at the outer layers of the SN matter far away from the self-induced (i.e., collective) oscillation zone. Because of the large spatial distance between the self-induced oscillation zone and the MSW oscillation zone, the MSW oscillation can happen essentially independently of the self-induced oscillations, with the latter simply pre-processing the neutrino flux of different flavors entering the MSW zone.

The effect of these various oscillation processes on the final fluxes of neutrinos of different flavors emerging from the SN would of course depend on several factors like initial luminosity, average energies and flux hierarchy of different flavors, and as these properties change from one emission phase to another the oscillation scenarios also change. In the initial accretion phase, due to the extreme matter densities, the collective effects are generally considered to be matter suppressed, and only the usual MSW effect is present [26, 27]. Although this remains to be conclusively established by further studies, we shall assume this to be the case in the present paper. Under this circumstance, the fluxes for the cases of normal ordering (NO) and inverted ordering (IO) of the neutrino mass hierarchy in the accretion phase are respectively given by (see, e.g., Ref. [28])

$$F_{\bar{\nu}_e}^{\text{NO}} = \cos^2 \theta_{12} F_{\bar{\nu}_e}^0 + \sin^2 \theta_{12} F_{\bar{\nu}_x}^0 \quad \text{and} \quad F_{\nu_e}^{\text{NO}} = F_{\nu_x}^0, \quad (3)$$

and

$$F_{\bar{\nu}_e}^{\text{IO}} = F_{\bar{\nu}_x}^0 \quad \text{and} \quad F_{\nu_e}^{\text{IO}} = \sin^2 \theta_{12} F_{\nu_e}^0 + \cos^2 \theta_{12} F_{\nu_x}^0. \quad (4)$$

In the longer cooling phase, due to smaller matter density, the dense matter suppression of collective effects is not present and multiple spectral splits due to self-induced conversions can happen in the collective oscillation region. This pre-processed flux will then go through the MSW oscillation. However, in the cooling phase the primary fluxes of different flavors of neutrinos are very similar (see Fig. 1). Under this circumstance, the self-induced conversions would tend to equilibrate the fluxes among different flavors. Indeed, such a trend towards equilibration of the cooling phase neutrino fluxes of different flavors has been observed in a number of numerical studies; for detailed discussions see, e.g., [26, 28, 29]. Therefore, oscillation effects on the final cooling phase neutrino flux emerging from the SN may be expected to be minimal, and so the fluxes of neutrinos of different flavors emerging from the SN in the final cooling phase may also be taken to be essentially given by the same expressions as for the accretion phase given in equations (3) and (4) above. Indeed, since in this paper we are interested only in the time integrated flux, the small differences in the emerging fluxes of different neutrino flavors in each emission phase get smeared out.

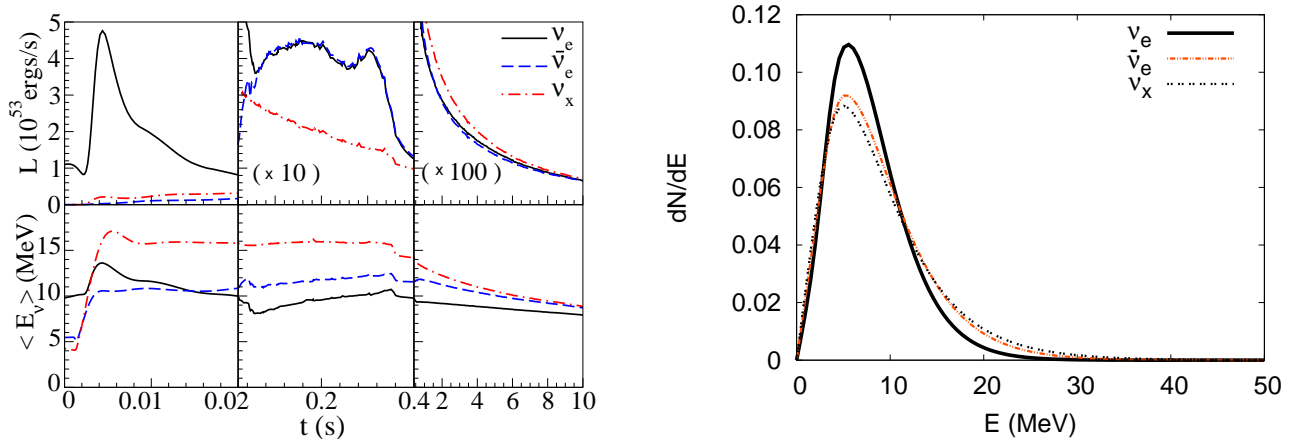


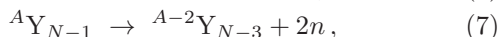
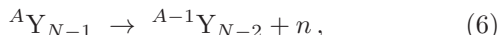
FIG. 1: Left: Temporal profiles of the neutrino luminosity (upper three panels) and average energy of the neutrinos (lower three panels) corresponding to the neutronization phase, accretion phase and cooling phase (from left to right, respectively) for different neutrino flavors, obtained from the results of the Basel/Darmstadt simulation [13] of a $18 M_{\odot}$ progenitor SN (From Ref. [20]). Right: The normalized time-averaged energy spectra of the neutrinos of different flavors.

III. THE NEUTRINO INDUCED CHARGED AND NEUTRAL CURRENT CROSS SECTIONS AND THE EMISSION OF NEUTRONS FROM NEUTRINO-EXCITED NUCLEI

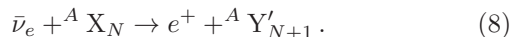
The supernova neutrinos can excite the nuclei ${}^A X_N$ of the detector material through the CC interaction producing the nuclei ${}^A Y_{N-1}$ by the reaction



The final nucleus gets de-excited by emitting particles or photons, and we are interested here in the reactions where one or more neutrons are emitted:



and so on. For ${}^{56}\text{Fe}$ detectors the excited nucleus is ${}^{56}\text{Co}$ whereas for ${}^{208}\text{Pb}$ it is ${}^{208}\text{Bi}$. In a similar fashion $\bar{\nu}_e$ through CC will produce positron and a different nucleus ${}^A Y'_{N+1}$ by the reaction



The nucleus ${}^A Y'_{N+1}$ if excited above one or two emission threshold will emit neutrons in competition with other particles and photons.

SN neutrinos can also excite detector nuclei through NC interactions. Neutrinos and antineutrinos of all three flavors can inelastically scatter from nuclei through NC interaction whereby the nucleus remains unchanged but goes to an excited state which can then de-excite by emitting neutrons.

The CC neutrino capture or NC scattering process and the subsequent emission of neutrons can be considered as a two-step process, and like in Kolbe and Langanke [9]

and Engel et al [10] we assume the two processes to be independent of each other. The first step involves calculating the CC or NC cross sections of neutrino interactions with the nuclei. During the interaction, an amount of energy $E_* \equiv E_f - E_i = E_{\nu} - E_{\ell}$, where E_i (E_f) is the energy of the initial (final) nucleus and E_{ν} (E_{ℓ}) is the energy of the incident neutrino (emerging lepton), is transferred to the final nucleus. This can excite a number of nuclear states in the final nucleus. The theoretical calculation of the cross section involves a multipole expansion of the current-current form of the weak interaction Hamiltonian and, assuming the lepton energies to be much greater than their masses, one relates the cross section to the nuclear transition operators of different multipole orders connecting the ground state of the target nucleus to the various (excited) states of the final nucleus [30–32]. This gives the ν -induced excitation spectrum, $\frac{d\sigma}{dE_*}(E_{\nu}, E_*)$, of the final nucleus, i.e., the differential cross section as a function of the excitation energy E_* of the final nucleus. We then calculate, in the second step, the cross section for emission of one-, two or more neutrons by the final nucleus by folding the ν -induced excitation spectrum of the final nucleus with the probabilities of decay of the nucleus through emission of specified number of neutrons as a function of the excitation energy of the nucleus. The latter is calculated using a suitable nuclear statistical model code discussed below.

For ν_e CC interactions, at typical SN neutrino energies of few tens of MeV for which $q = |\mathbf{q}| \rightarrow 0$ limit (\mathbf{q} being the 3-momentum transfer to the nucleus) is applicable, the cross section is dominated by contributions from the allowed transitions to the isobaric analog state (IAS) and the Gamow-Teller (GT) resonance states in the final nucleus. The allowed contribution to the (ν_e, e^-) differential cross section in the $q \rightarrow 0$ limit can thus be written in terms of the effective Fermi and GT transition strengths

as [31, 33, 34]

$$\frac{d\sigma_{\nu_e}^{\text{CC,allowed}}}{dE_*}(E_\nu, E_*) = \frac{G_F^2 \cos^2 \theta_c}{\pi} p_e E_e F(Z+1, E_e) \times (S_F(E_*) + S_{\text{GT}_-}(E_*)), \quad (9)$$

where m_e , p_e and E_e are the mass, momentum and energy of the emitted electron, respectively, G_F is the Fermi constant, θ_C is the Cabibbo angle,

$$S_F(E_*) = \frac{1}{2J_i + 1} \left| \langle J_f \parallel \sum_{k=1}^A \tau_+(k) \parallel J_i \rangle \right|^2 \quad (10)$$

and

$$S_{\text{GT}_-}(E_*) = \frac{(g_A^{\text{eff}})^2}{2J_i + 1} \left| \langle J_f \parallel \sum_{k=1}^A \tau_+(k) \sigma(k) \parallel J_i \rangle \right|^2 \quad (11)$$

are the Fermi and GT strength distributions, respectively, as functions of the excitation energy $E_* = E_f - E_i = E_\nu - E_e$ of the final nucleus, J_i and J_f represent the angular momentum of the initial and final nucleus, respectively, τ_+ is the operator that converts a neutron to a proton, and σ are the standard Pauli spin matrices. The quantity (g_A^{eff}) is the ratio of the effective axial vector to vector coupling constants of the nucleon in the $q \rightarrow 0$ limit, whose value for the “bare” nucleon is 1.26 [31, 33]. The factor $F(Z+1, E_e)$ is the correction factor to account for the distortion of the outgoing electron wave function due to the Coulomb field of the final state nucleus.

For $p_{e,\text{eff}} R \ll 1$, where $p_{e,\text{eff}} = \left[(E_e - V(0))^2 - m_e^2 \right]^{1/2}$ with $V(0) = (3/2)e^2 Z_f / R$, (eZ_f and R being the charge and radius of the final nucleus, respectively), the Coulomb correction factor can be represented by the Fermi function [35],

$$F(Z, E) = 2(1 + \gamma_0)(2p_e R)^{2(\gamma_0 - 1)} \frac{|\Gamma(\gamma_0 + iy)|^2}{|\Gamma(2\gamma_0 + 1)|^2} \exp(\pi y), \quad (12)$$

where $\gamma_0 = (1 - Z^2 \alpha^2)^{1/2}$ and $y = \alpha Z E_e / p_e$, with α the fine structure constant.

The $\bar{\nu}_e$ CC cross section is similar where the final state lepton is a positron instead of electron, and the Fermi function then takes care of the distortion of the positron wave function due to the repulsion effect of the final nucleus. Also, one replaces the operator τ_+ above by τ_- which transforms a proton to a neutron.

For the NC scattering of neutrino, the analog of Fermi transition only contributes to elastic scattering [33], and the allowed contribution to the cross section for inelastic scattering (that involves energy transfer to the target nucleus) in the $q \rightarrow 0$ limit is governed by the NC GT (the so-called GT_0) strength [33]

$$S_{\text{GT}_0}(E_*) = \frac{(g_A^{\text{eff}})^2}{2J_i + 1} \left| \langle J_f \parallel \sum_{k=1}^A \frac{1}{2} \tau_3(k) \sigma(k) \parallel J_i \rangle \right|^2, \quad (13)$$

giving the allowed contribution to the (ν, ν') NC induced excitation spectrum of the final nucleus in the $q \rightarrow 0$ limit as

$$\frac{d\sigma_{\nu}^{\text{NC,allowed}}}{dE_*}(E_\nu, E_*) = \frac{G_F^2}{\pi} E_{\nu'}^2 S_{\text{GT}_0}(E_*), \quad (14)$$

where $E_{\nu'} = E_\nu - E_*$ is the energy of the final neutrino. In equation (13), $\frac{1}{2}\tau_3$ is the third (“z”-) component of the isospin operator.

For small but non-zero momentum transfer q , in addition to the allowed contributions to the cross sections discussed above, there would be additional small, but in general non-negligible, contributions to the cross sections due to the forbidden transitions originating from terms linear in q [31].

In the case of $^{56}\text{Fe}(\nu_e, e^-)^{56}\text{Co}$ reaction, with the ground state of ^{56}Fe being a $J = 0$ state, the allowed transitions connect to the 0^+ and 1^+ states of ^{56}Co . We add to that the smaller contributions coming from the first forbidden transitions to the 1^- and 2^- states in ^{56}Co which are mostly at higher excitation energies than the ones connected by the allowed transitions. For the allowed transitions, we use the GT strength distribution from large-scale shell model calculations using the monopole corrected KB3 interaction [36] which is very successful in reproducing the spectra of nuclei in the iron region. The calculated GT strengths GT_- and GT_+ for the $^{56}\text{Fe}(\nu_e, e^-)^{56}\text{Co}$ and $^{56}\text{Fe}(\bar{\nu}_e, e^+)^{56}\text{Mn}$ reactions obtained by Caurier *et al.* [36] compare well with the values extracted from $L = 0$ forward angle (p, n) and (n, p) cross sections, respectively, with some small differences appearing at the high energy end. The strength distributions for the forbidden transitions to 1^- and 2^- states of ^{56}Co are obtained by unfolding the contributions of these transitions to the neutrino-spectrum-averaged $^{56}\text{Fe}(\nu_e, e^-)^{56}\text{Co}$ differential cross section as a function of the ^{56}Co excitation energy given in Ref. [34] for the KARMEN experiment’s decay-at-rest ν_e spectrum [37].

For the NC case, we use the strength distribution calculated by Toivanen *et al.* [38] which includes both the $\Delta T=0$ and 1 resonances though the strength for transitions to the higher isospin is very small.

With the ν -induced excitation spectrum of the final nucleus obtained as above, the total CC or NC cross section as a function of the incident neutrino energy E_ν is obtained as

$$\sigma^{\text{CC(NC)}}(E_\nu) = \int \frac{d\sigma^{\text{CC(NC)}}}{dE_*}(E_\nu, E_*) dE_*, \quad (15)$$

and the CC and NC cross sections for emission of one-, two- or three neutrons as

$$\sigma_{1n(2n)(3n)}^{\text{CC(NC)}}(E_\nu) = \int \frac{d\sigma^{\text{CC(NC)}}}{dE_*}(E_\nu, E_*) P_{1n(2n)(3n)}(E_*) dE_*, \quad (16)$$

where $\frac{d\sigma^{\text{CC(NC)}}}{dE_*}(E_\nu, E_*)$ is the relevant ν -induced excitation spectrum of the final nucleus, and $P_{1n}(E_*)$, $P_{2n}(E_*)$,

$P_{3n}(E_*)$ are the probabilities for emission of one-, two- and three neutrons, respectively, as functions of the excitation energy of the final nucleus.

Finally, the number of neutrons produced as a function of incident neutrino energy is given by

$$\frac{dN_n^{\text{CC(NC)}}}{dE_\nu}(E_\nu) = N_T \Phi_\nu(E_\nu) \sum_{k=1}^3 k \sigma_{kn}^{\text{CC(NC)}}(E_\nu), \quad (17)$$

where $\sigma_{kn}^{\text{CC(NC)}}$ (for $k = 1, 2, 3$) are given by equation (16), $\Phi_\nu(E_\nu)$ is the time-integrated flux spectrum (number per unit area per unit energy) of the SN neutrinos falling on the detector, and N_T is the total number of target detector nuclei.

The calculations of the neutron emission probabilities for ^{56}Fe were done using the fusion-evaporation code PACE4 [39] originally developed by Gavron [40], which is based on a modified version of Monte Carlo statistical model calculations using angular momentum projection at each stage of de-excitation of the nucleus. The results for the neutron emission probabilities from excited ^{56}Fe and ^{56}Co nuclei as functions of excitation energy are shown in Figure 2. These are used for the calculations of emission of neutrons through NC interaction of neutrinos of all flavors and CC interaction of ν_e , respectively, with ^{56}Fe nuclei. Note that the excitation energy threshold for emission of one neutron (1n) from ^{56}Fe is 11.2 MeV whereas it is 25 MeV for two neutrons (2n). Three neutrons are emitted only beyond the high excitation energy of 38 MeV. In the case of excited ^{56}Co nuclei resulting from CC interaction of ν_e with ^{56}Fe , the 1n emission starts from excitation energy of 11 MeV and 2n from 16 MeV. Three neutrons are emitted only beyond an excitation energy of 35 MeV. Results for CC interaction of $\bar{\nu}_e$ with ^{56}Fe resulting in excited ^{56}Mn are also treated in a similar manner.

For the case of ^{208}Pb we directly use the 1n and 2n emission cross sections given by Engel, McLaughlin and Volpe [10] which have the weak interaction cross section folded in for both CC and NC. These calculations were carried out by the coordinate space Skyrme-Hartree-Fock method in a 20 fm box and then by a version of RPA using the same Skyrme interaction in the basis of Hartree-Fock states. The threshold for 1n and 2n emission for ^{208}Pb are 6.9 and 15.0 MeV, respectively.

IV. RESULTS

Pb detectors

The number of neutrons emitted per kTon of lead for CC interaction of supernova ν_e 's as a function of the neutrino energy for the time-integrated neutrino fluxes given by the B/D simulation results discussed above in Section II is given in the form of a histogram of bin size 5 MeV in Figure 3 for both Normal Order (NO) and Inverted Order

(IO) of neutrino mass hierarchy assuming 100% detection efficiency. The bin-wise contributions of 1n and 2n events are also shown. Contributions from 3n events are negligible. These take into account the matter effect as described in Sec. II. From the right panel of Fig. 1, which shows the time-integrated energy spectra for all three neutrino species, we see that the maximum in the energy distribution of the electron neutrinos is below 10 MeV beyond which the spectrum falls rapidly. However, the CC cross section increases rapidly with neutrino energy, roughly as E_ν^2 . In addition, the probability of one neutron emission from excited ^{208}Bi nucleus starts increasing and taking non-zero values beyond the 1n emission threshold of 6.9 MeV. Together, these effects result in a maximum for the number of neutrons emitted in the energy bin of 25-30 MeV for the ν_e case both for NO and IO of the mass hierarchy. The total number of neutrons emitted in the case of NO is 154, with 1n and 2n events contributing 107 and 47 neutrons, respectively. The corresponding numbers for the case of IO are 117, 84 and 33, respectively.

We note here that the above numbers are significantly smaller than earlier estimates (see, e.g., [7]) based on older SN models [14, 15] which have different neutrino energy spectra compared to those given by the B/D simulations considered here and also involve different neutrino flavor conversion scenarios. One observes that for ν_e the average energy in the B/D simulation is always less than 15 MeV and below 10 MeV for the longest lasting cooling phase (see Fig. 1). Similarly, the ν_x average energies are always lower than 17 MeV and lower than 14 MeV during the entire cooling phase. With both ν_e and ν_x having lower average energies than those in earlier simulations, the number of neutrons for both NO and IO are smaller than the earlier estimates (even with 100% detection efficiency and substantial flavor mixing assumed here), and so is the difference between the numbers for NO and IO cases.

We also mention here that, since a detector such as the HALO [11] may be able to distinguish between the 1n and 2n events, the ratio of 1n and 2n events (which would be independent of the total neutrino flux) may yield interesting spectral information on the SN neutrino flux [12]. This, however, is subject to several uncertainties, and we will not discuss this further in this paper.

The number of events due to CC interactions of the SN $\bar{\nu}_e$'s ($^{208}\text{Pb} + \bar{\nu}_e \rightarrow ^{208}\text{Tl} + e^+$) are orders of magnitude smaller than those due to ν_e 's mainly due to the fact that beta transitions of protons to neutrons are strongly suppressed due to Pauli blocking of the neutron single particle states. Thus the process has negligibly small contribution and we do not consider the $\bar{\nu}_e$ events.

For the NC events all the six species of supernova neutrinos contribute and there is no difference in the results for the two mass hierarchies. The total number of neutrons emitted for NC interactions per kTon of lead is 30, with 21 from 1n events and the rest from 2n events. The histogram of the number of neutrons emitted as a

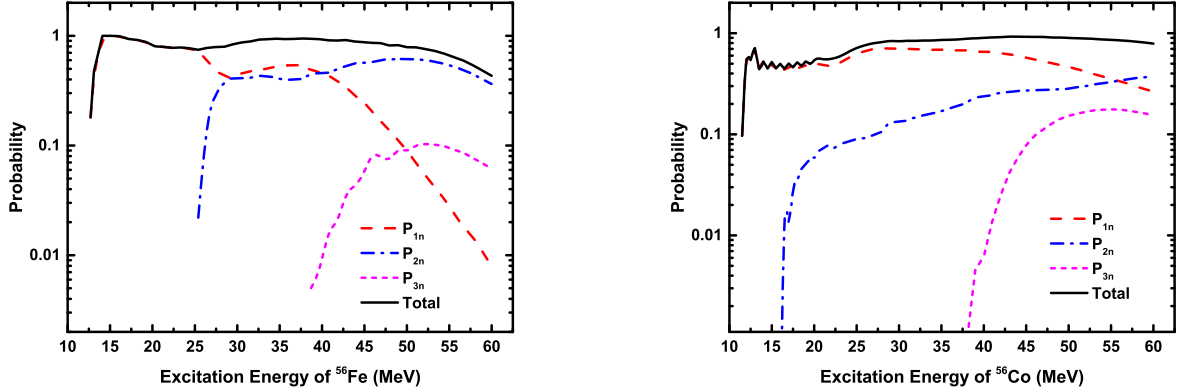


FIG. 2: The one-, two- and three neutron emission probabilities (P_{1n} , P_{2n} , and P_{3n} , respectively) of excited ^{56}Fe nucleus (left) and excited ^{56}Co nucleus (right) as a function of the excitation energy.

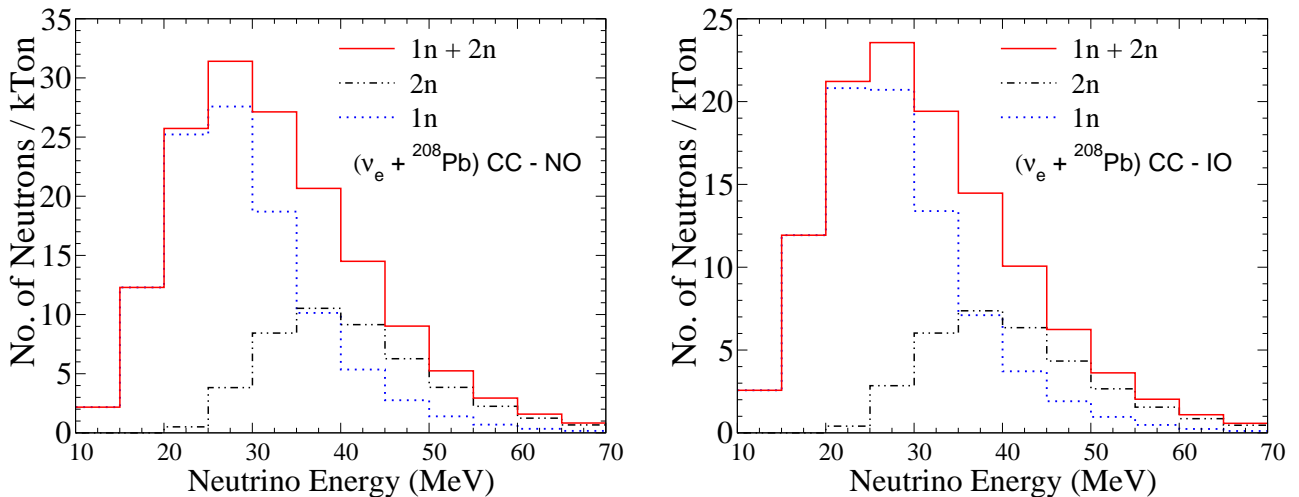


FIG. 3: Number of neutrons emitted due to ν_e CC interactions per kTon of ^{208}Pb as function of neutrino energy for Normal Order (NO) (left panel) and Inverted Order (IO) (right panel) of neutrino mass hierarchy. “1n” and “2n” indicate neutrons from one- and two-neutron emission events, respectively.

function of neutrino energy with a bin size of 5 MeV is shown in Fig. 4. These numbers are also smaller than the previous estimates [7].

It is clear that the number of neutrons produced per kTon of ^{208}Pb is dominated by the CC events, a result already known from earlier studies; see, e.g., Ref. [12]. From the numbers obtained above, the number of neutrons produced through NC interactions is $\sim 16\%$ (20%) of the total number of produced neutrons in the case of NO (IO) of mass hierarchy. Thus, in absence of the capability to identify the CC induced events (through identification of the accompanying e^-) it will not be possible for a ^{208}Pb detector by itself to determine the fraction of the μ and τ flavored neutrinos in the total SN neutrino flux.

Fe detectors

The total CC cross section (σ^{CC}) for $^{56}\text{Fe}(\nu_e, e^-)^{56}\text{Co}$ and total NC cross section (σ^{NC}) for $^{56}\text{Fe}(\nu, \nu')^{56}\text{Fe}$ as functions of neutrino energy (E_ν), with the GT strength distributions as described in Sec. III including the contributions coming from the first forbidden transitions, are given in Table I. The corresponding one- and two-neutron emission cross sections, $\sigma_{1n}^{\text{CC(NC)}}$ and $\sigma_{2n}^{\text{CC(NC)}}$, are also tabulated.

The total $^{56}\text{Fe}(\nu_e, e^-)^{56}\text{Co}$ CC cross section has been calculated by several authors using various microscopic approaches. In Figure 5 we show a comparison of our results with those given in Refs. [9, 41, 42], for example. It is seen that, while all the results show a rapidly rising cross section with neutrino energy, there is con-

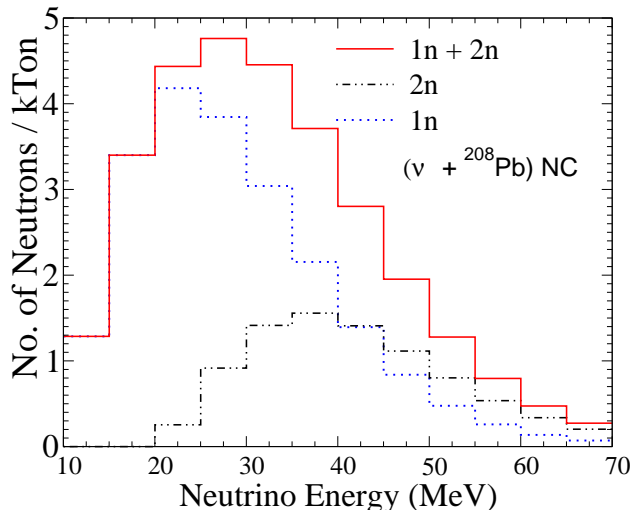


FIG. 4: Number of neutrons emitted due to NC interaction of all six species of neutrinos per kTon of ^{208}Pb as function of neutrino energy. “1n” and “2n” indicate neutrons from one- and two-neutron emission events, respectively.

E_ν (MeV)	$^{56}\text{Fe}(\nu_e, e^-)^{56}\text{Co}$			$^{56}\text{Fe}(\nu, \nu')^{56}\text{Fe}$		
	σ^{CC} (cm^2)	σ_{1n}^{CC} (cm^2)	σ_{2n}^{CC} (cm^2)	σ^{NC} (cm^2)	σ_{1n}^{NC} (cm^2)	σ_{2n}^{NC} (cm^2)
10	3.12E-42	0.0	0.0	1.37E-43	1.31E-44	0.0
15	1.31E-41	2.89E-43	0.0	2.23E-42	2.80E-43	0.0
20	3.65E-41	2.50E-42	9.33E-46	7.86E-42	1.21E-42	0.0
25	7.43E-41	7.22E-42	1.26E-44	1.73E-41	2.99E-42	1.16E-49
30	1.28E-40	1.50E-41	9.65E-44	3.05E-41	5.70E-42	2.77E-45
35	2.02E-40	2.80E-41	4.83E-43	4.74E-41	9.42E-42	3.68E-44
40	3.04E-40	4.94E-41	1.60E-42	6.82E-41	1.42E-41	1.49E-43
45	4.45E-40	8.45E-41	4.08E-42	9.27E-41	2.01E-41	3.88E-43
50	6.39E-40	1.40E-40	8.72E-42	1.21E-40	2.71E-41	8.13E-43
55	9.03E-40	2.23E-40	1.66E-41	1.53E-40	3.53E-41	1.49E-42
60	1.26E-39	3.43E-40	2.88E-41	1.89E-40	4.47E-41	2.49E-42

TABLE I: The total CC cross section (σ^{CC}) for $^{56}\text{Fe}(\nu_e, e^-)^{56}\text{Co}$ and total NC cross section (σ^{NC}) for $^{56}\text{Fe}(\nu, \nu')^{56}\text{Fe}$ as functions of neutrino energy (E_ν). The corresponding one- and two neutron emission cross sections, $\sigma_{1n}^{\text{CC(NC)}}$ and $\sigma_{2n}^{\text{CC(NC)}}$, are also given.

siderable amount of differences amongst the results of different theoretical calculations. Our results are close to those of Kolbe and Langanke [9] (K-L) at lower energies while being close to the results of [42](Paar et al) at relatively higher energies. At all energies, the cross section values obtained in [41] (L-V) are the largest, while those given by Paar et al [42] are the smallest, the two sets of values differing by almost a factor of 5 at some energies. Our results lie bracketed within those of K-L and Paar et al at all energies.

The $^{56}\text{Fe}(\nu_e, e^-)^{56}\text{Co}$ cross section has been measured, although with a low precision, by the KARMEN experiment [37]. The spectrum-averaged value

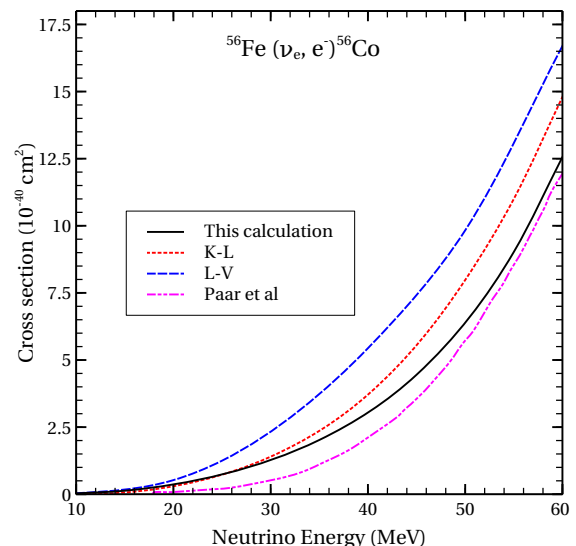


FIG. 5: Total $^{56}\text{Fe}(\nu_e, e^-)^{56}\text{Co}$ cross section as a function of neutrino energy. For comparison, the cross sections obtained in Refs. [9] (K-L), [41] (L-V) and [42] (Paar et al) are also shown.

of the cross section for the decay-at-rest (DAR) ν_e spectrum, $n(E_\nu)_{\text{DAR}} = 96E_\nu^2(M_\mu - 2E_\nu)/M_\mu^4$ (where M_μ is the muon mass) was measured to be $\langle\sigma(^{56}\text{Fe}(\nu_e, e^-)^{56}\text{Co})\rangle_{\text{DAR}} = [2.51 \pm 0.83(\text{stat.}) \pm 0.42(\text{syst.})] \times 10^{-40} \text{cm}^2$. With our ν_e CC cross section values given in Table I, we get a value of $1.98 \times 10^{-40} \text{cm}^2$ for the same DAR spectrum-averaged cross section, which is quite consistent within experimental errors with the KARMEN measured value.

Our results for the total NC cross section for the process $^{56}\text{Fe}(\nu, \nu')^{56}\text{Fe}$ given in Table I also compare reasonably well with those given in Table VI of K-L [9], for example.

The number of neutrons emitted per kTon of ^{56}Fe as a function of incoming neutrino energy, calculated using equation (17) with the $^{56}\text{Fe}(\nu_e, e^-)^{56}\text{Co}$ CC one- and two neutron emission cross sections given in Table I, is shown in Fig. 6 in the form of histograms of 5 MeV energy bins for both NO and IO mass hierarchies. It is seen that, unlike in the case of ^{208}Pb , essentially all the neutrons are from 1n events, with 2n events giving negligibly small contribution in the case of ^{56}Fe . The total number of neutrons emitted is ~ 3 and 2 for NO and IO, respectively. As the neutron emission threshold for ^{56}Co is ~ 11.0 MeV, only the tail of the neutrino energy distribution contributes. Also the Fermi strength at the Isobaric Analog State (IAS) around 4 MeV and most of the GT giant resonance distribution has no contribution as the one neutron emission probability is zero or almost zero up to ~ 12.5 MeV. As a result the forbidden transitions become relatively more important ($\sim 24\%$ and 22% of the GT strengths for NO and IO cases, respectively). However, even including those, the total number of neutron events turns out to be very small.

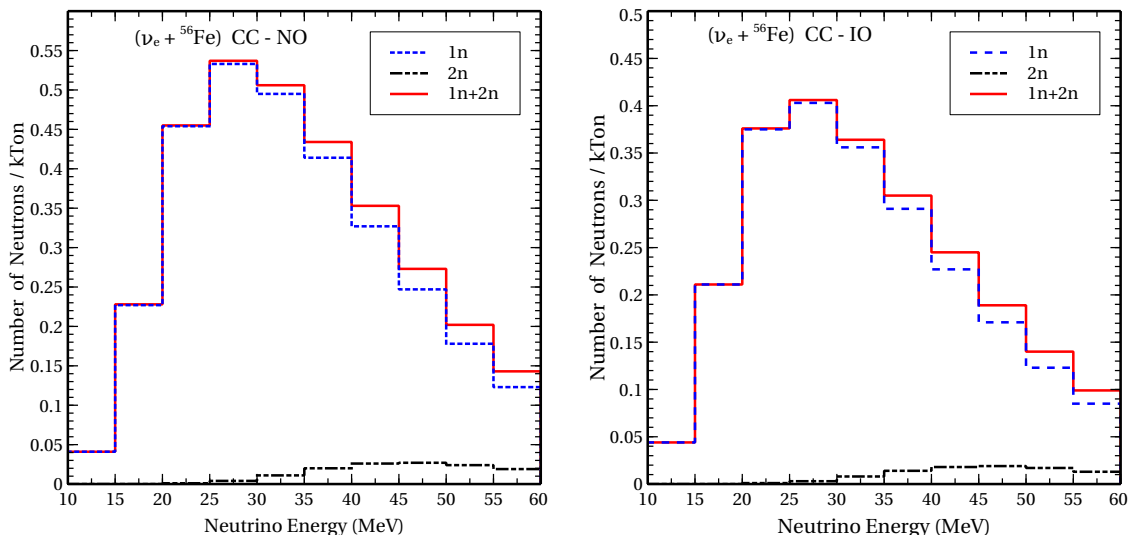


FIG. 6: Number of neutrons emitted due to ν_e CC interactions per kTon of ^{56}Fe as function of neutrino energy for Normal Order (NO) (left panel) and Inverted Order (IO) (right panel) of neutrino mass hierarchy. “1n” and “2n” indicate neutrons from one- and two-neutron emission events, respectively.

The $\bar{\nu}_e$ CC process, $^{56}\text{Fe}(\bar{\nu}_e, e^+)^{56}\text{Mn}$, gives negligibly small number of neutrons emitted by the excited ^{56}Mn nucleus. Firstly, the total GT_+ strength is experimentally seen to be ~ 2.8 with the theoretical shell model number being 2.7 [36], whereas the total GT_- strength corresponding to the ν_e CC reaction $^{56}\text{Fe}(\nu_e, e^-)^{56}\text{Co}$ discussed above is 9.9 experimentally [36] and 9.3 from theoretical calculations. But even more important is the fact that the nucleus ^{56}Mn has the one-neutron emission threshold above 8 MeV and almost all the GT_+ strength lies below the excitation energy of 8 MeV.

For NC interactions, the histogram of the sum of the number of neutrons emitted due to all the six species of neutrinos is shown in Fig. 7. Again, the contribution from 2n events is negligibly small. The total number of neutrons emitted is ~ 5 . Without the additional contribution from ($\Delta T = 1$) resonance, the number is ~ 4 . This again is the reflection of the fact that the 1n emission threshold for ^{56}Fe is 8 MeV whereas the NC excitation strength (GT_0) distribution has only the tail part of the resonance beyond 8 MeV [38]. We note here that, in contrast to the situation for ^{208}Pb , the total number of neutrons produced per kTon in the case of ^{56}Fe is dominated by those produced through the NC interactions. Specifically, for ^{56}Fe , the NC induced neutrons constitute $\sim 62\%$ (71%) of the total number of neutrons produced in the case of NO (IO) mass hierarchy.

Comparison of ^{208}Pb and ^{56}Fe as detector materials

Although in the above discussions we have not at all considered the issues of specific detector configurations and detection efficiencies of specific kinds of detectors, it is already clear from the results presented above that,

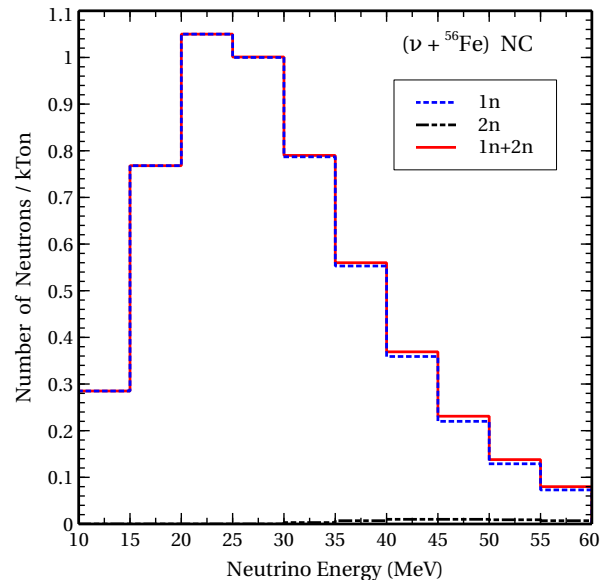


FIG. 7: Number of neutrons emitted due to NC interaction of all six species of neutrinos per kTon of ^{56}Fe as function of neutrino energy. “1n” and “2n” indicate neutrons from one- and two-neutron emission events, respectively.

per kTon of material, ^{56}Fe gives the number of emitted neutrons lower by more than an order of magnitude compared to ^{208}Pb both for CC and NC interactions. This is due to two reasons. Firstly, the total Gamow-Teller strength for ν_e CC cross section roughly scales as $N - Z$, N and Z being the number of neutrons and protons, respectively, in the nucleus. This neutron excess is 44 for ^{208}Pb and only 4 for ^{56}Fe . Also, the neutron emission thresholds for both ^{208}Pb and ^{208}Bi are a few MeV lower

compared to those of ^{56}Fe and ^{56}Mn . As a result the contribution of most of the allowed strengths for both CC and NC cannot make any contribution for ^{56}Fe but they do for ^{208}Pb . Thus, as a detector material ^{208}Pb is more efficient than ^{56}Fe for observing supernova neutrinos.

However, as clear from the discussions above, a ^{208}Pb detector would be primarily sensitive to ν_e 's through CC interactions, with neutrons produced through NC interactions of ν_e , $\bar{\nu}_e$, ν_x and $\bar{\nu}_x$ comprising in total $\sim 20\%$ or less of all the produced neutrons. In contrast, in a ^{56}Fe detector, most ($\gtrsim 60\%$) of all the neutrons produced should be of NC origin. Thus, without the ability to separately identify the CC induced events (through identification of the accompanying e^-) in either detector, simultaneous detection of SN neutrinos in a ^{208}Pb and a sufficiently large ^{56}Fe detector, together with the knowledge of the expected fractions of total numbers of CC and NC events in each detector as discussed above, may, in principle, allow a determination of the fractions of μ and τ flavored neutrinos in the total SN neutrino flux.

At the present time, however, neutrino cross sections on both iron and lead at the relevant neutrino energies are still rather uncertain, with no precise measurements of these cross sections being currently available, and so a proper assessment of the feasibility of the above approach will have to await the availability of more precisely determined neutrino cross sections on lead as well as iron. Also, realistic estimates of the minimum sizes of the lead and iron detectors that would allow extraction of meaningful information on the ν_μ and ν_τ components of the SN neutrino flux will require a more detailed analysis, than has been attempted here, involving the relevant statistical as well as systematic uncertainties — the latter including those due to uncertainties in the relevant cross sections.

V. SUMMARY AND CONCLUSIONS

We have presented the results of our study of the possibility of detecting SN neutrinos with ^{56}Fe and ^{208}Pb detectors through detection of neutrons emitted by the excited nuclei resulting from the interaction of SN neutrinos with the nuclei of these detector materials. In doing this, we have used the results of the most recent state-of-the-art Basel/Darmstadt simulations [13] for the supernova neutrino fluxes and average energies, which typically yield closer fluxes among different neutrino flavors and lower average energies compared to those given by earlier simulations [14, 15]. Specifically, we have used

the simulation results of the Basel/Darmstadt simulations for a $18M_\odot$ progenitor SN at a distance of 10 kpc. Our results for the numbers of neutron events per kTon of detector material are found to be significantly lower than those estimated in previous studies which were based on earlier simulations of SN neutrino emission. It will be of interest to study the implications of this result for the possibility of effectively distinguishing between the neutrino mass hierarchies using SN neutrino detection (see, e.g., Refs. [43, 44]).

We also make the observation that, while ^{208}Pb would be a better detector material than ^{56}Fe in terms of the total number of neutrons produced per kTon of detector mass, $\sim 80\%$ or more of the produced neutrons in the case of ^{208}Pb arise from CC interactions of ν_e , whereas neutrons produced in ^{56}Fe are dominated by those produced through NC interactions of all the six ν plus $\bar{\nu}$ species. Thus, a sufficiently large ^{56}Fe detector — large enough to compensate for the overall smaller ν - ^{56}Fe cross sections compared to ν - ^{208}Pb cross sections — can be a good NC detector for SN neutrinos. For example, the proposed 50 kTon iron calorimeter (ICAL) [45] detector, though primarily designed for studying neutrino properties using the relatively higher energy (multi-GeV) atmospheric neutrinos, can also be a good NC detector of SN neutrinos if it can be appropriately instrumented with suitable neutron detectors. Thus, simultaneous detection of SN neutrinos in a ^{208}Pb and a ^{56}Fe detector can, in principle, provide an estimate of the relative fractions of the ν_e and the other five neutrino species in the SN neutrino flux, which would be a good probe of the SN neutrino production as well as flavor oscillation scenarios. It will be interesting to carry out more detailed analysis involving relevant statistical and systematic uncertainties — the latter including those due to (currently somewhat large) uncertainties in neutrino cross sections on lead and iron — to derive estimates of the minimum lead and iron detector sizes that would allow extraction of statistically significant information on the ν_μ and ν_τ components of the SN neutrino flux.

Acknowledgment: One of us (SC) thanks Tobias Fischer for providing the numerical data for the temporal profiles of the luminosities and average energies of neutrinos of different flavors for the Basel/Darmstadt SN simulations used in this paper. SC also acknowledges partial support by the Deutsche Forschungsgemeinschaft through Grant No. EXC 153 (“Excellence Cluster Universe”) and by the European Union through the “Initial Training Network Invisibles,” Grant No. PITN-GA-2011-289442.

[1] G. G. Raffelt, *Ann. Rev. Nucl. Part. Sci.* **49**, 163 (1999).
 [2] H. Duan and J.P. Kneller, *J. Phys. G: Nucl. Part. Phys.* **36**, 113201 (2009).

[3] K. Hirata *et al.* [KAMIOKANDE-II Collaboration], *Phys. Rev. Lett.* **58**, 1490 (1987); *Phys. Rev. D* **38**, 448 (1988).

- [4] R.M. Bionta *et al.*, Phys. Rev. Lett. **58**, 1494 (1987); C.B. Bratton *et al.*, Phys. Rev. D **37**, 3361 (1988).
- [5] E.N. Alekseev, L.N. Alekseeva, I.V. Krivosheina and V.I. Volchenko, Phys. Lett. B **205**, 209 (1988).
- [6] V.L. Dadykin *et al.* JETP Lett. **45**, 593 (1987); M. Aglietta *et al* Europhys. Lett. **3**, 1315 (1987).
- [7] K. Scholberg, Ann. Rev. Nucl. Part. Sci. **62**, 81 (2012).
- [8] D.B. Cline *et al.*, Astrophys. Lett. Commun. **27**, 403 (1990); Phys. Rev. D **50**, 720 (1994); C.K. Hargrove *et al.*, Astropart. Phys. **5**, 183 (1996); P.F. Smith, Astropart. Phys. **8**, 27 (1997); G.M. Fuller, W.C. Haxton, and G.C. McLaughlin, Phys. Rev. D **59**, 085005 (1999); S. Elliott, Phys. Rev. C **62**, 065802 (2000); J.J. Zach, A.S.J. Murphy, D. Marriott and R.N. Boyd, Nucl. Instrum. Meth. A **484**, 194 (2002); R.N. Boyd, A.S.J. Murphy, and R.L. Talaga, Nucl. Phys. A **718**, 222 (2003).
- [9] E. Kolbe and K. Langanke, Phys. Rev. C **63** 025802 (2001)
- [10] J. Engel, G.C. McLaughlin and C. Volpe, Phys. Rev. D **67**, 013005 (2003).
- [11] C.A. Duba *et al.*, J. Phys. Conf. Ser. **136**, 042077 (2008).
- [12] D. Väänänen and C. Volpe, JCAP **10** (2011) 019 [arXiv:1105.6225].
- [13] T. Fischer, S.C. Whitehouse, A. Mezzacappa, F.-K. Thielemann and M. Liebendorfer, Astron. Astrophys. **517**, A80 (2010) [arXiv:0908.1871].
- [14] T. Totani, K. Sato, H.E. Dalhed and J.R. Wilson, Astrophys. J. **496** 216 (1998).
- [15] J. Gava, J. Kneller, C. Volpe and G.C. McLaughlin, Phys. Rev. Lett. **103**, 071101 (2009).
- [16] B. Müller, H.-T. Janka and A. Marek, Astrophys. J. **756**, 84 (2012) [arXiv:1202.0815]; B. Müller, A. Marek, H.-T. Janka, and H. Dimmelmeier, ASP Conf. Ser. **459**, 137 (2012) [arXiv:1112.1920].
- [17] T.M. Undagoitia and L. Rauch, J. Phys. G: Nucl. Part. Phys. **43**, 013001 (2016) [arXiv:1509.08767].
- [18] C.J. Horowitz, K.J. Coakley, and D.N. McKinsey, Phys. Rev. D **68**, 023005 (2003).
- [19] D.Z. Freedman, Phys. Rev. D **9**, 1389 (1974); D.Z. Freedman, D.N. Schramm, and D.L. Tubbs, Ann. Rev. Nucl. Part. Sci. **27**, 167 (1977).
- [20] S. Chakraborty, P. Bhattacharjee and K. Kar, Phys. Rev D **89**, 013011 (2014).
- [21] K. Abe et al. (XMASS collaboration), arXiv:1604.01218.
- [22] R. F. Lang, C. McCabe, S. Reichard, M. Selvi and I. Tamborra, arXiv:1606.09243.
- [23] M. T. Keil, G.G. Raffelt and H.T. Janka, Astrophys. J. **590** 971 (2003).
- [24] H. Duan, G.M. Fuller and Y.-Z. Qian, Ann. Rev. Nucl. Part. Sci. **60**, 569 (2010) [arXiv:1001.2799].
- [25] A. Mirizzi, I. Tamborra, H. T. Janka, N. Saviano, K. Scholberg, R. Bollig, L. Hudepohl and S. Chakraborty, Riv. Nuovo Cim. **39** (2016) no.1-2, 1.
- [26] S. Chakraborty, T. Fischer, A. Mirizzi, N. Saviano and R. Tomas, Phys. Rev. Lett. **107**, 151101 (2011).
- [27] S. Chakraborty, T. Fischer, A. Mirizzi, N. Saviano and R. Tomas, Phys. Rev D **84** 025002 (2011).
- [28] E. Borriello, S. Chakraborty, A. Mirizzi, P.D. Serpico and I. Tamborra, Phys. Rev. D **86**, 083004 (2012) [arXiv:1207.5049].
- [29] T. Fischer, G. Martínez-Pinedo, M. Hempel, and M. Liebendorfer, Phys. Rev. D **85**, 083003 (2012).
- [30] J.D. Walecka, Semileptonic weak interactions in nuclei, in *Muon Physics*, Vol.2: Weak Interactions, ed. V.W. Hughes and C.S. Wu (Academic, New York, 1975).
- [31] T. Kuramoto, M. Fukugita, Y. Kohyama, and K. Kubodera, Nucl. Phys. A **512**, 711 (1990).
- [32] E. Kolbe, K. Langanke, G. Martinez-Pinedo and P. Vogel, J. Phys. G **29**, 2569 (2003).
- [33] G.M. Fuller, W.C. Haxton, and G.C. McLaughlin, Phys. Rev. D **59**, 085005 (1999).
- [34] E. Kolbe, K. Langanke and G. Martinez-Pinedo, Phys. Rev. C **60**, 052801 (1999).
- [35] J. Engel, Phys. Rev. C **57**, 2004 (1998).
- [36] E. Caurier, K. Langanke, G. Martinez-Pinedo and F. Nowacki, Nucl. Phys. A **653**, 439 (1999).
- [37] R. Maschuw, Prog. Part. Nucl. Phys. **40**, 183 (1998).
- [38] J. Toivanen et al., Nucl. Phys. A **694**, 395 (2001).
- [39] <http://lise.nsl.msui.edu/pace4.html>; O.B. Tarasov and D. Bazin, Nucl. Instrum. Meth. B **204**, 174 (2003).
- [40] A Gavron, Phys. Rev. C **21**, 230 (1980).
- [41] R. Lazauskas and C. Volpe, Nucl. Phys. A **792**, 219 (2007).
- [42] N. Paar, D. Vretenar and P. Ring, J. Phys. G: Nucl. Part. Phys. **35**, 014058 (2008).
- [43] D. Vale and N. Paar, AIP Conf. Proc. **1681**, 050011 (2015) [arXiv:1406.2584].
- [44] D. Vale, T. Rauscher and N. Paar, JCAP **02** (2016) 007 [arXiv:1509.07342].
- [45] The ICAL collaboration, arXiv:1505.07380.